Cellular/Molecular

Surface Traffic of Dendritic $Ca_V1.2$ Calcium Channels in Hippocampal Neurons

Valentina Di Biase,[1] Petronel Tuluc,[1] Marta Campiglio,[1] Gerald J. Obermair,[1] Martin Heine,[2] and Bernhard E. Flucher[1]

[1]Department of Physiology and Medical Physics, Medical University of Innsbruck, 6020 Innsbruck, Austria and [2]Leibniz Institute for Neurobiology, 39118 Magdeburg, Germany

In neurons L-type calcium currents function in gene regulation and synaptic plasticity, while excessive calcium influx leads to excitotoxicity and neurodegeneration. The major neuronal $Ca_V1.2$ L-type channels are localized in clusters in dendritic shafts and spines. Whereas $Ca_V1.2$ clusters remain stable during NMDA-induced synaptic depression, L-type calcium currents are rapidly downregulated during strong excitatory stimulation. Here we used fluorescence recovery after photobleaching (FRAP), live cell-labeling protocols, and single particle tracking (SPT) to analyze the turnover and surface traffic of $Ca_V1.2$ in dendrites of mature cultured mouse and rat hippocampal neurons, respectively. FRAP analysis of channels extracellularly tagged with superecliptic pHluorin ($Ca_V1.2$-SEP) demonstrated ~20% recovery within 2 min without reappearance of clusters. Pulse–chase labeling showed that membrane-expressed $Ca_V1.2$-HA is not internalized within1 h, while blocking dynamin-dependent endocytosis resulted in increased cluster density after 30 min. Together, these results suggest a turnover rate of clustered $Ca_V1.2$s on the hour time scale. Direct recording of the lateral movement in the membrane using SPT demonstrated that dendritic $Ca_V1.2$s show highly confined mobility with diffusion coefficients of ~0.005 $\mu m^2 s^{-1}$. Consistent with the mobile $Ca_V1.2$ fraction observed in FRAP, a ~30% subpopulation of channels reversibly exchanged between confined and diffusive states. Remarkably, high potassium depolarization did not alter the recovery rates in FRAP or the diffusion coefficients in SPT analyses. Thus, an equilibrium of clustered and dynamic $Ca_V1.2$s maintains stable calcium channel complexes involved in activity-dependent cell signaling, whereas the minor mobile channel pool in mature neurons allows limited capacity for short-term adaptations.

Introduction

L-type calcium channels (LTCCs) and NMDA receptors are the main sources of calcium influx in the postsynaptic compartment of neurons. In physiological conditions, activity-induced calcium influx through either channel regulates gene expression and synaptic and homeostatic plasticity. In pathological conditions it leads to hyperexcitability, excitotoxicity, and neurodegeneration. Specifically, LTCCs function in signaling to the nucleus (Graef et al., 1999; Deisseroth et al., 2003; Dolmetsch, 2003; Oliveria et al., 2007), long-term potentiation, spatial memory (Moosmang et al., 2005), and heterosynaptic plasticity (Lee et al., 2009; Rose et al., 2009). Like NMDA receptor signaling (Barria and Malinow, 2005), activation of CaMKII in calcium nanodomains near the mouth of LTCCs is critical for nuclear signaling (Lee et al., 2009; Rose et al., 2009). On the other hand, excessive L-type currents leading to global calcium signals have been implicated in neurodegenerative disease (Stanika et al., 2010), and blocking LTCCs effectively reduces neuronal cell death in stroke and Parkinson disease (Korenkov et al., 2000; Schurr, 2004; Day et al., 2006; Chan et al., 2007). Thus, the tight control of LTCC levels in the membrane and their localization in postsynaptic signaling complexes are of central importance for the proper function of neurons.

$Ca_V1.2$ is the most abundant LTCC in mammalian brain (Hell et al., 1993; Clark et al., 2003; Schlick et al., 2010). It is localized in small clusters in dendritic shafts and spines (Obermair et al., 2004), both in extrasynaptic locations as well as in postsynaptic signaling complexes with adrenergic receptors, AKAP79/150, protein kinase-A, and calcineurin (Davare et al., 2001). These $Ca_V1.2$ clusters appear to be very stable and independent of the highly plastic signaling complex of the postsynaptic density. Neither deletion of known scaffold binding sites in the $Ca_V1.2$ C-terminus nor NMDA-induced disruption of the postsynaptic density affected the integrity of dendritic $Ca_V1.2$ clusters in well differentiated hippocampal neurons (Weick et al., 2003; Di Biase et al., 2008). In young neurons however, sustained depolarization or activation of NMDA receptors reduce L-type calcium currents and cause internalization of $Ca_V1.2$ channels. This response involves dynamin-dependent endocytosis and has been suggested to protect neurons from excitotoxic cell death (Green et al., 2007).

Received May 9, 2011; revised July 28, 2011; accepted Aug. 3, 2011.

Author contributions: V.D.B. and B.E.F. designed research; V.D.B., P.T., M.C., and M.H. performed research; G.J.O. contributed unpublished reagents/analytic tools; V.D.B., P.T., and M.H. analyzed data; V.D.B. and B.E.F. wrote the paper.

This work was supported by the Austrian Science Fund Grants T443-B18 to V.D.B. and P20059-B05 and W1101 to B.E.F.; LSA-Project 04035 and Deutsche Forschungsgemeinschaft Grant HE-3604/2-1 to M.H. We thank Dr. Martin Offterdinger of the Biooptics Facility for technical assistance at the confocal microscope; Benedikt Nimmervoll, Heidemarie Wickborn, and Sabine Opitz for providing primary cultures of hippocampal neurons; and Sabrina Hassler and Annika Lenuweit for excellent technical assistance.

The authors declare no competing financial interests.

Correspondence should be addressed to either of the following: Bernhard E. Flucher, Fritz-Pregl Strasse 3, Medical University of Innsbruck, 6020 Innsbruck, Austria, E-mail: bernhard.e.flucher@i-med.ac.at or Martin Heine, Brenneckestrasse 6, Leibniz Institute for Neurobiology Magdeburg, 39118 Magdeburg, Germany, E-mail: martin.heine@lin-magdeburg.de.

DOI:10.1523/JNEUROSCI.2300-11.2011

 0270-6474/11/3113682-13$15.00/0

Nevertheless, the turnover rates and membrane dynamics of LTCCs are hitherto unknown. Therefore, we combined fluorescence recovery after photobleaching (FRAP) analysis, live cell-labeling protocols, and single particle tracing (SPT) to analyze the turnover and surface traffic of $Ca_V1.2$ in dendrites of mature cultured hippocampal neurons. Our results demonstrate the coexistence of stably clustered and mobile $Ca_V1.2$ channels and provide the first quantitative data on diffusion rates and modes of mobility of a voltage-gated calcium channel in neurons. The low turnover and mobility of clustered $Ca_V1.2$ channels indicate that $Ca_V1.2$ signaling in CNS is not subject to rapid modulation by channel internalization. Whereas the dynamic channel population provides a potential mechanism for short-term adaptations, its small pool size in mature, electrically active neurons, however, affords little capacity for further activity-induced downregulation of channel density.

Materials and Methods

Primary cultures of mouse and rat hippocampal neurons. Low-density cultures of hippocampal neurons were prepared from 16.5-d-old embryonic BALB/c mice or from 18-d-old embryonic Sprague Dawley rats of either sex as described previously (Goslin and Banker, 1998; Obermair et al., 2003, 2004). Briefly, dissected hippocampi were dissociated by trypsin treatment and trituration. Neurons were plated on poly-L-lysine-coated glass coverslips in 60 mm culture dishes at a density of 3500 cells/cm^2 or 100–200 $\times$ 10^3 cells/ml for mice and rat cultures, respectively. After plating, cells were allowed to attach for 3–4 h before transferring the coverslips neuron-side-down into a 60 mm culture dish with a glial feeder layer. Neurons and glial feeder layer were cultured in serum-free Neurobasal medium (Invitrogen) supplemented with GlutaMax and B27 (Invitrogen). All experiments with the exception of SPT were performed on mouse neurons.

Transfection of hippocampal neurons. Plasmids were introduced into mouse neurons at 6 days *in vitro* (DIV) using Lipofectamine 2000-mediated transfection (Invitrogen) as described by Obermair et al. (2004). For single transfection (pβA-$Ca_V1.2$-SEP or pβA-$Ca_V1.2$-HA) experiments, 1.5 μg total DNA were used. For cotransfection (pβA-eGFP plus pβA-$Ca_V1.2$-HA) experiments, 2 μg of total DNA were used at a molar ratio of 1:2. Cells were processed for experiments 11–14 d after transfection. Rat hippocampal neurons were transfected using the calcium phosphate method as described previously (Dresbach et al., 2003).

Plasmids. Generation of pβA-eGFP and pβA-$Ca_V1.2$-HA ($Ca_V1.2$-HA: GenBank accession no. M67515; Altier et al., 2002) was described previously (Obermair et al., 2004). The pβA-$Ca_V1.2$-SEP construct was generated by cloning superecliptic-pHluorin (SEP) into the respective position of the hemagglutinin (HA) tag at the S5-H5 loop of the pβA-$Ca_V1.2$-HA as follows. SEP was isolated from the pcDNA3.1 plasmid (kindly provided by Prof. J. Henley, University of Bristol, Bristol, UK) by PCR. The forward primer was designed to introduce a MluI restriction site and a thrombin cleavage site (ctggttccgcgtggatcc) followed by two glycines (ggagga) 5′ to the SEP sequence. The reverse primer introduced two glycines, a second thrombin cleavage site followed by the nucleotide sequence (nt) 2092–2097 of the $Ca_V1.2$-HA cDNA. A second PCR fragment was generated from the pβA-$Ca_V1.2$-HA (nt 2092–2392), introducing a silent mutation (g to a) at the base pair 2110 to delete the MluI restriction site. The two PCR generated fragments were then fused by SOE-PCR (where SOE is splicing by overlap extension). The amino acid sequence of the insertion fragment reads ***FDEMQTR***-*LVPRGS*-GG-**SEP**-GG-*LVPRGS*-***FDEMQTR***, where italics represent thrombin cleavage sites, **SEP** symbolizes the SEP sequence, and the bold italics represent a repetition of nt 2035–2055 of the S5-H5 loop in the $Ca_V1.2$-HA cDNA. Finally, the SOE-SEP-fragment and pβA-$Ca_V1.2$-HA were MluI and SalI digested and subsequently ligated. The postsynaptic markers Homer1C-DsRed and PSD95-mCherry were gifts from D. Choquet (University of Bordeaux, Bordeaux, France).

Antibodies and fluorescent probes. Antibodies and fluorescent probes used were as follows: rat anti-HA (monoclonal, clone 3F10, Roche Diagnostics, 1:100 for immunolabeling, 1:50 for SPT); mouse anti-Synaptotagmin1-Oyster550 (SySy, Synaptic Systems, Goettingen, 1:200); monoclonal mouse anti GFP (Roche); goat anti-rat Alexa Fluor 594 (1:4000, Invitrogen); transferrin-Alexa Fluor 488 (Tf-488, Invitrogen, 50 μg/μl); phalloidin-Alexa Fluor 594 (Invitrogen, 1:300).

Surface staining of $Ca_V1.2$-HA. In pulse–chase surface-labeling experiments, 18- to 20-d-old $Ca_V1.2$-HA transfected neurons were incubated with anti-HA for 10 min. Zero, 5, 15, 30, and 60 min after removing the antibody, coverslips were rinsed in PBS and fixed with 4% paraformaldehyde for 10 min. To block endocytosis, neurons cotransfected with $Ca_V1.2$-HA and enhanced GFP (eGFP) were simultaneously incubated with anti-HA (1:100) and 80 μM Dynasore (Sigma) in neuronal medium for 15 and 30 min at 37°C. Subsequently, cultures were washed and fixed with paraformaldehyde for 10 min. In all surface-labeling experiments after fixation, neurons were washed with PBS for 30 min, blocked with 5% goat serum for 30 min, and labeled with anti-rat Alexa Fluor 594 (1:4000, 1 h). Coverslips were mounted in *p*-phenylenediamine glycerol to retard photobleaching (Flucher et al., 1993) and observed with an Axio Imager microscope (Carl Zeiss) using 63×, 1.4 NA oil-immersion objective lens. Images were recorded with cooled CCD camera (SPOT; Diagnostic Instruments).

Quantification of $Ca_V1.2$-HA clusters. Fourteen-bit gray scale images of anti-HA (red channel) and eGFP (green channel) were acquired and analyzed as described previously (Di Biase et al. 2008). Briefly, corresponding images were aligned and the eGFP image was used to select the regions of interest (ROIs) for measuring the average gray values (fluorescence intensity) and numbers of $Ca_V1.2$-HA clusters per spine and length of dendritic shaft (density) with MetaMorph software (Universal Imaging). In Dynasore experiments, ROIs (5 pixels diameter) were placed over each $Ca_V1.2$-HA cluster to measure the fluorescence intensity. The average gray values of the clusters were background subtracted. Density and intensities of $Ca_V1.2$-HA clusters were expressed as percentage of control.

Quantification of colocalization of $Ca_V1.2$-HA clusters with Tf-488. Fourteen-bit gray-scale images of the red (HA) and green channel (Tf-488) were acquired. Dendritic regions of corresponding images were 2D deconvolved (MetaMorph). Colocalization was analyzed according to the center of mass coincidence-based method, and the Pearson's coefficient was calculated using the JACoP plugin (Bolte and Cordelières, 2006) in ImageJ (W. S. Rasband, ImageJ, National Institutes of Health, Bethesda, MD; http://rsb.info.nih.gov/ij/, 1997–2007). Results are expressed as percentage of $Ca_V1.2$-HA objects colocalizing with Tf-488.

FRAP analysis. FRAP was performed on 13- to 21-d-old $Ca_V1.2$-SEP-transfected neurons using an SP-5 confocal microscope (Leica Microsystems) equipped with a 63×, 1.4 NA water-immersion lens at 37°C in an incubation chamber (EMBLEM). Neurons were mounted in a Ludin chamber in Tyrode's physiological solution containing the following (in mM): 130 NaCl, 2.5 KCl, 2 $CaCl_2$, 2 $MgCl_2$, 10 HEPES, 30 glucose. Fluorescence was excited using the 488 nm line of the argon laser and recorded at a bandwidth of 500–550 nm at an acquisition rate of 1.5 Hz. For imaging in the pre-bleach and post-bleach phases the laser was set to ~10% of the initially adjusted laser power (70%). One rectangular 10-μm-long ROI along the dendritic branch was photobleached by scanning with the 488 nm line of argon laser at 100% intensity. For longer post-bleach acquisition protocols, an additional five frames were acquired every 3 min. FRAP recordings in depolarized condition were performed in neurons in 60 mM KCl bath solution 15 min before recordings. Average fluorescence in ROIs was measured, background subtracted, and corrected for overall photobleaching in each time frame. The average fluorescence within the ROI was double normalized so that the pre-bleach intensity was set to 1 and the first frame after photobleaching to 0 and plotted as function of time. The analysis of fluorescence was performed using LAS AF (Leica Microsystems) and MetaMorph software.

Single particle tracking. To label $Ca_V1.2$-SEP channels, quantum dots (QDs) with 655 nm fluorescence emission (QD-655) [highly cross-adsorbed goat F(ab′)$_2$ anti-mouse IgG conjugate (heavy + light chains), 0.1 μM, Invitrogen] were precoated with mouse anti-GFP (0.5 μg) in 10 μl of PBS for 30 min and blocked with casein (onefold dilution, Vector Labs) for 15 min. $Ca_V1.2$-SEP-transfected neurons were incubated with

precoated QDs at a final concentration of 0.1 nM for 5 min at 37°C, followed by four 30 s washes in HEPES-buffered extracellular solution containing 0.5% BSA. Cells were then mounted in a closed chamber and analyzed at the microscope. For labeling, $Ca_V1.2$-HA channels neurons were first incubated with anti-HA (Roche, 1:50) in culture medium for 15 min followed by a 5 min incubation with QD-655 goat $F(ab')_2$ anti-rat in cultured medium at 37°C. After washing, cells were mounted in an open chamber and used for imaging experiments for up to 20 min at 37°C.

Combined single particle tracking and fluorescence microscopy. Time lapse recordings of QD-labeled $Ca_V1.2$-HA relative to Homer1C-DsRed were acquired at 37°C in an open chamber mounted onto an inverted microscope (Axio Observer, Zeiss) equipped with a 60×/1.35 NA or 100×/1.3 NA objective. Recordings of QD-labeled $Ca_V1.2$ channels relative to $Ca_V1.2$-SEP clusters, PSD-95mCherry, and Synaptotagmin1-Oyster550 were conducted at an Olympus microscope (BX50) equipped with a spinning disk (CSU X1, Yokogawa) using a 100×/1.3 NA objective. At both instruments images were acquired with a back-illuminated, thinned CCD camera (QuantEM, Roper Scientific). Fluorescence of QDs and synaptic PSD95-mCherry or Homer1C-DsRed was excited by a xenon lamp using excitation filter HQ500/20X and 560RDF55, respectively. Emitted fluorescence was acquired through filters HQ560/80M and 655WB20, respectively. Time lapse recordings of QDs were obtained with an integration time of 30 ms with up to 1000–2000 consecutive frames. QD-labeled $Ca_V1.2$ channels were followed on randomly selected dendritic regions for up to 20 min. Z-stacks of $Ca_V1.2$-SEP clusters and synaptic markers where acquired before and after QD recording. QD fixed to the coverslip allowed compensation for mechanical drifts of the stage.

Channel tracking and analysis. The tracking of single QDs was performed using a homemade software based on MATHLAB (MathWorks). Single QDs were identified by their blinking fluorescent emission and their diffraction-limited signals. The trajectories of QDs bound to $Ca_V1.2$-SEP and $Ca_V1.2$-HA channels were reconstructed with a point accuracy of ~60 nm. The blinking properties of QDs did not allow the recording of trajectories as a continuum. Therefore, subtrajectories of the same QD-bound channels were reconnected when the displacement of the QDs between two frames was 1–2 pixels and the maximal dark periods of 25 frames between blinking events. To analyze the motion parameters of single channels, mean squared displacement (MSD) curves were calculated and plotted over time for reconnected trajectories of at least 100 frames. The resolution limit for diffusion was 0.001 $\mu m^2\ s^{-1}$, obtained from recordings of fixed QDs. Diffusion coefficients were calculated by linear fit of the first four points of the MSD plots versus time on the dendrites, axons, and inside or outside the $Ca_V1.2$-SEP clusters and synapses (Saxton, 1995). The confinement index was calculated using custom software as described by Sergé et al. (2002). For QDs in transit between the $Ca_V1.2$-SEP clusters or synaptic compartments, the dwell time index was calculated as follows: time spent in $Ca_V1.2$-SEP clusters or synapses/(total acquisition time × number of exits from $Ca_V1.2$-SEP clusters or synapses) as described by Charrier et al. (2010). For labeled channels that did not leave the synapse or cluster during the recording period, the dwell time index was set to 1.

Electrophysiology. Calcium currents were recorded using the whole-cell patch-clamp technique. Patch pipettes were pulled from borosilicate glass (Harvard Apparatus), fire-polished (Microforge MF-830, Narishige), and had resistances of 1.5–3 MΩ when filled with the following (in mM): 145 cesium aspartate, 2 $MgCl_2$, 10 HEPES, 0.1 Cs-EGTA, 2 Mg-ATP (pH 7.4 with CsOH) (Tanabe et al., 1990; Kasielke et al., 2003). The bath solution contained the following (in mM): 10 $CaCl_2$, 145 tetraethylammonium chloride, 10 HEPES (pH 7.4 with tetraethylammonium hydroxide). Currents were recorded with an Axopatch 200B amplifier (Molecular Devices) controlled by pClamp software (version 8.0, Molecular Devices). Linear leak and capacitive currents were digitally subtracted with a P/4 prepulse protocol. The current–voltage dependence was fitted according to Equation 1:

$$I = G_{max} \cdot (V - V_{rev})/1(1 + \exp(-(V - V_{1/2})/k)), \quad (1)$$

where G_{max} is the maximum conductance of the L-type calcium channels, V_{rev} is the extrapolated reversal potential of the calcium current, $V_{1/2}$ is the potential for half-maximal conductance, and k is the slope. The voltage dependence of the Ca^{2+} conductance was fitted according to a Boltzmann distribution:

$$G = G_{max}/(1 + \exp(-(V - V_{1/2})/k)). \quad (2)$$

Statistical analysis. Statistical significance of normalized data was calculated using ANOVA and *t* test (Microsoft Excel 2007) in pulse chase surface labeling and Dynasore experiments. Nonparametric statistics was used to calculate the statistical significance of FRAP and SPT analysis, using χ^2 test and Kruskal-Wallis followed by a Dunn's test and a Mann–Whitney test, respectively (GraphPad). Analyses were performed on 15–25 neurons from at least three different experiments and at least three separate culture preparations. All data are reported as mean ± SEM, SD, or median ± interquartile range (IQR, 25–75%) as indicated in the text. Graphs and figures were generated using Origin 7.5, Igor Pro, GraphPad Prism, and Adobe Photoshop 8.0 software.

Results

FRAP analysis revealed a major immobile and a minor mobile population of membrane-expressed $Ca_V1.2$-SEP

FRAP, fluorescent recovery after photobleaching, was used to determine the mobility of channels in dendrites of hippocampal neurons. If fluorescently tagged channels within a bleached membrane patch are continuously exchanged with unbleached channels from outside that region, recovery of the fluorescence labeling pattern would be expected. To limit the FRAP analysis to surface-expressed $Ca_V1.2$ channels, we generated a $Ca_V1.2$ construct tagged with SEP, superecliptic pHluorin, in the extracellular loop between transmembrane helix IIS5 and the pore loop. SEP is a pH-sensitive GFP analog (Miesenböck et al., 1998; Sankaranarayanan et al., 2000; Ashby et al., 2004). When excited at 488 nm it is strongly fluorescent at neutral pH, whereas its fluorescent emission is abolished at pH 6. Therefore, $Ca_V1.2$-SEP exposed to the neutral extracellular environment is brightly visible, while $Ca_V1.2$-SEP contained in acidic cytoplasmic compartments shows little to no fluorescence.

Figure 1*A* shows a representative confocal image of dendrites of 18 DIV hippocampal neurons expressing $Ca_V1.2$-SEP before, immediately after, and 20 min after photobleaching. The intrinsic SEP fluorescence is distributed in clusters along the dendritic shafts and in spines, resembling the distribution patterns described previously for surface-expressed $Ca_V1.2$-HA and for the endogenous $Ca_V1.2$ (Figs. 2–4) (Obermair et al., 2004). This indicates that $Ca_V1.2$-SEP is normally inserted and targeted in the dendritic plasma membrane of hippocampal neurons. Conversely, normal clustering of $Ca_V1.2$-SEP observed with the intrinsic SEP fluorescence confirms the surface organization observed in live cell immunolabeling experiments with $Ca_V1.2$-HA and excludes the possibility that clusters are induced by antibody cross-linking. Two scans with the full intensity of the 488 nm wavelength laser line caused a dramatic drop of fluorescence in the bleached region (yellow box, ~26 μm^2), while $Ca_V1.2$-SEP clusters outside the bleached region remained unaltered. Twenty minutes after bleaching the clusters outside the bleached region were still mostly unchanged, whereas those in the bleached region had not reappeared (Fig. 1*B*). Comparing the distribution of clusters in unbleached regions at the beginning and the end of the experiment aided by a subtraction image (Fig. 1*C*) further demonstrates that over 20 min most clusters persisted and did not change their position (arrows). Interestingly, isolated clusters disappeared (filled arrowheads, white in subtraction image) and others appeared (open arrowheads, black in subtraction image) during the 20 min live cell observation.

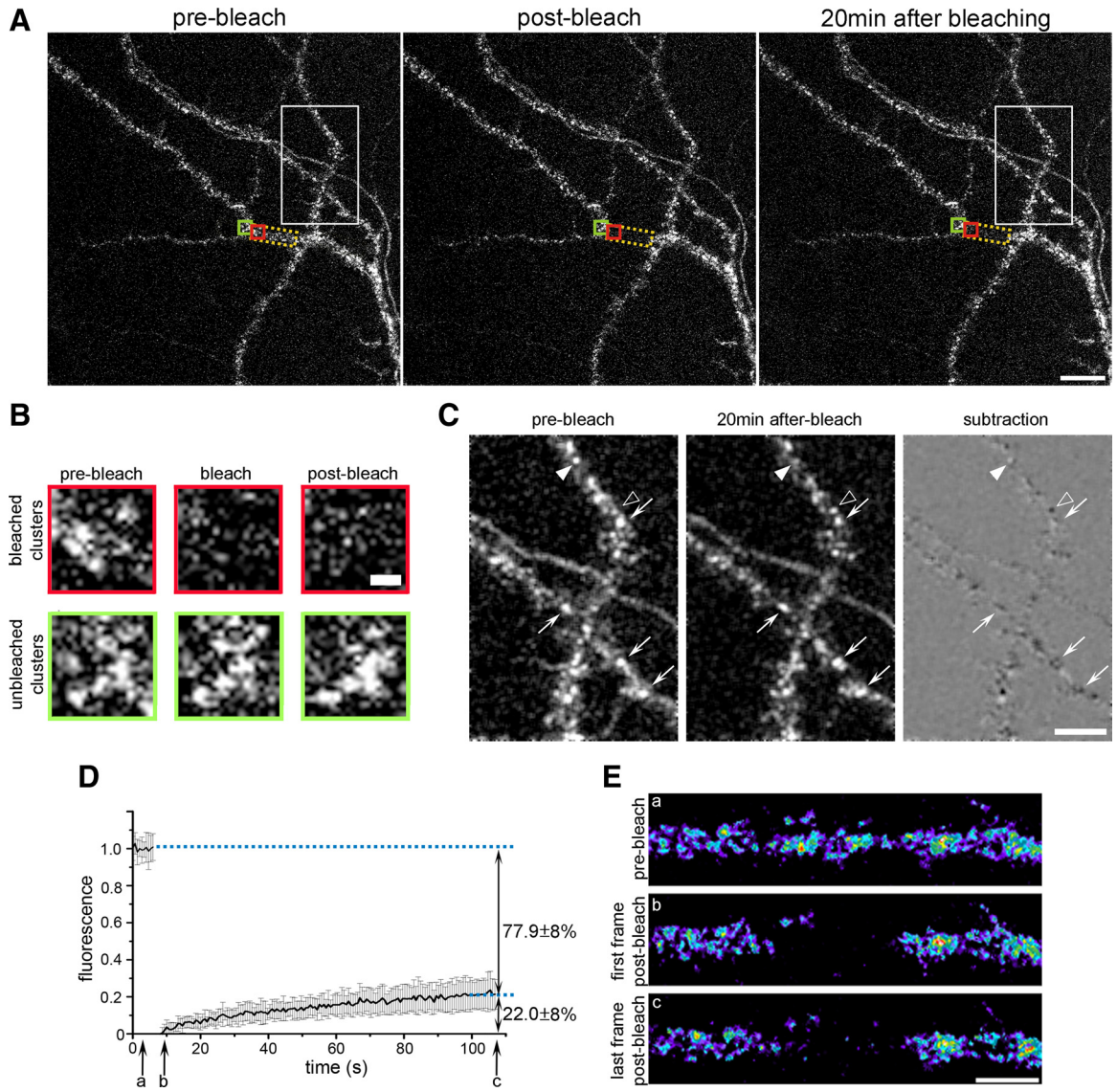

Figure 1. FRAP analysis reveals a stably clustered and a minor mobile fraction of $Ca_V1.2$-SEP in dendrites of hippocampal neurons. ***A***, Representative image of a branched dendrite expressing $Ca_V1.2$-SEP before, immediately after, and 20 min after photobleaching (area indicated by yellow frame). Over 20 min the staining of $Ca_V1.2$-SEP clusters showed little changes outside and little recovery of fluorescence inside the bleached region. Scale bar, 10 μm. ***B***, Enlargement of $Ca_V1.2$-SEP clusters in an unbleached (green frame) and a bleached (red frame) region of the dendrite in ***A*** at the three time points. Partial recovery of fluorescence 20 min after bleaching is not accompanied by a reappearance of the clusters. Scale bar, 1 μm. ***C***, Enlargement of unbleached area in ***A*** (white frame) and corresponding subtraction image demonstrate that most $Ca_V1.2$-SEP clusters did not change (arrows), while a few clusters disappeared (filled arrowheads) or appeared (open arrowheads) during the 20 min observation time. Scale bar, 5 μm. ***D***, Average normalized FRAP curve from experiments in which the fluorescence recovery was recorded for 99 s at 1.5 Hz (mean $\pm$ SD; $N = 17$ recordings from three experiments). On average, the $Ca_V1.2$-SEP fluorescence in the bleached dendritic segments recovered by 22.8 $\pm$ 8%. ***E***, Representative frames (***a***–***c***) of a $Ca_V1.2$-SEP expressing dendrite from the FRAP experiment in ***C*** show that the recovering fraction of channels were not clustered. Scale bar, 5 μm.

Quantitative FRAP analysis for 120 s at a sampling rate of 1.5 Hz revealed on average a 22.8 $\pm$ 8% fluorescence recovery within 2 min (Fig. 1*D*), indicating the existence of a mobile population of $Ca_V1.2$-SEP channels. However, comparison of the pre-bleach images with the last images of recordings again confirmed that this recovery of overall fluorescence was not accompanied by a reappearance of $Ca_V1.2$-SEP clusters (Fig. 1*E*). The fact that clusters did not reappear within the recording period or even after 20 min suggests that the mobile fraction of $Ca_V1.2$-SEP channels in dendrites of hippocampal neurons exists outside the clusters. Conversely, the clustered channels can readily account for the major immobile population of $Ca_V1.2$-SEP channels. To further test this notion, the turnover rates of the calcium channels in the clusters needed to be determined.

The turnover rate of $Ca_V1.2$ channels in dendritic clusters of cultured hippocampal neurons greatly exceeds one hour

The number of proteins in the membrane is the result of the balance between insertion and internalization (Fig. 2*D*). Relative changes of the rates of these two actions may cause activity-induced changes in membrane expression of neuronal membrane proteins. To satisfactorily explain changes in membrane expression by these mechanisms, the turnover rates ought to be in the same order of magnitude as the observed changes in membrane expression. Although L-type calcium channels were suggested to be subject to rapid activity-induced internalization (Green et al., 2007), turnover rates of $Ca_V1.2$ channels in neurons are not known. Because our FRAP analysis (Fig. 1) indicated that within 2 min partial recovery of $Ca_V1.2$-SEP fluorescence did not

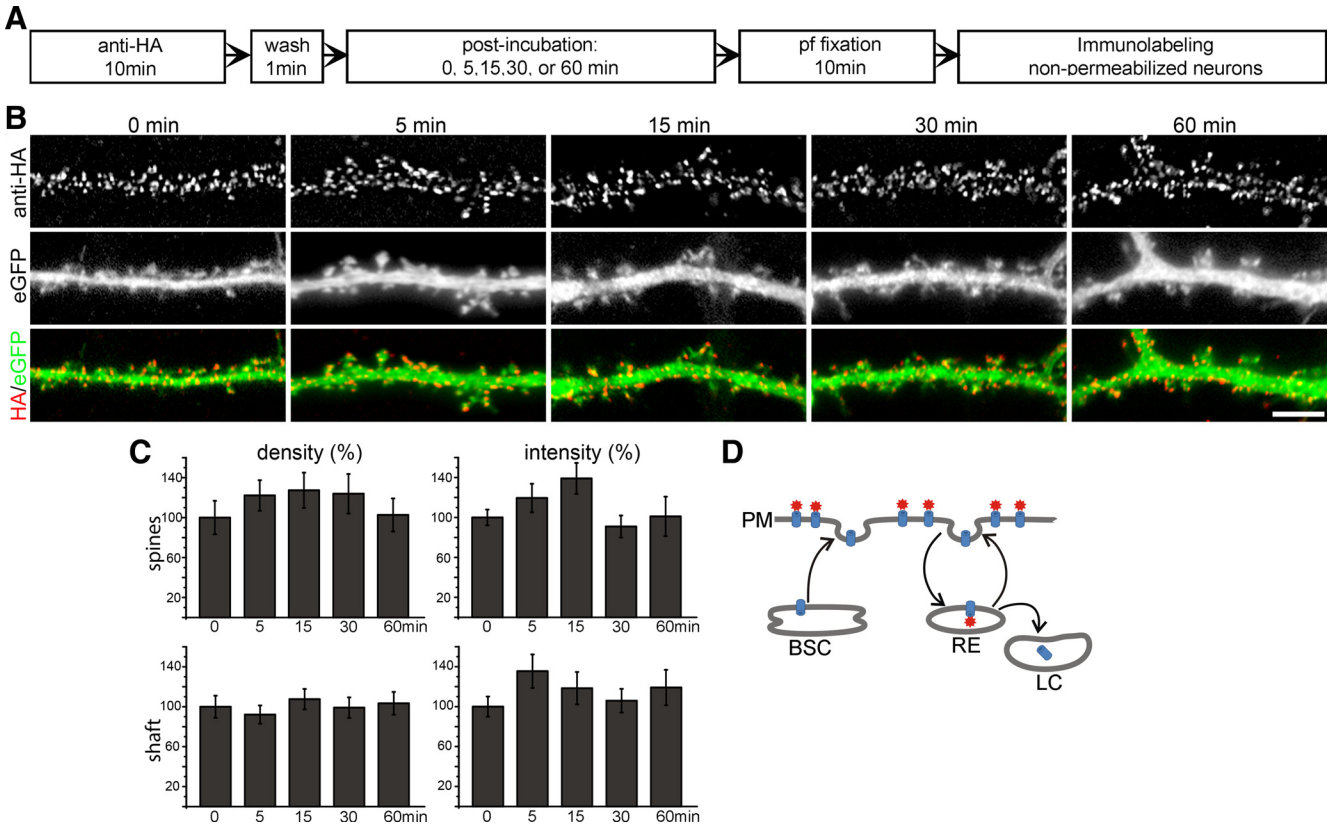

Figure 2. Surface-labeled $Ca_V1.2$-HA clusters in living hippocampal neurons are not internalized within 60 min. ***A***, Experimental workflow. pf, Paraformaldehyde. ***B***, $Ca_V1.2$-HA- and eGFP-cotransfected neurons were live cell labeled with anti-HA for 10 min and fixed 0, 5, 10, 15, 30, or 60 min after removing the antibody (antibody and subsequent incubation at 37°C). The secondary antibody was applied to unpermeabilized neurons to exclusively label channels remaining at the surface. Coexpressed soluble eGFP outlines the dendrite morphology. At all time points $Ca_V1.2$-HA clusters show a similar localization on dendritic shafts and spines. Scale bar, 5 μm. ***C***, Quantification of the density (number of clusters per spine or per μm^2 of dendritic shaft) and the fluorescence intensity (average gray value) of $Ca_V1.2$-HA clusters expressed as percentage of surface labeling at the 0 time point. Over 60 min no significant changes were observed (one-way ANOVA, $p = 0.17–0.88$). ***D***, Schematic turnover pathways of membrane proteins. PM, Plasma membrane; BSC, biosynthetic compartment; RE, recycling endosomes; LC, lysosomal compartment. Bar graphs, mean ± SEM; $N = 12–14$ analyzed dendritic segments in three separate experiments.

involve the restoration of channel clusters, we decided to determine the turnover rate of $Ca_V1.2$ in clusters over a longer period and to investigate the potential role of channel insertion and internalization in the maintenance of stable $Ca_V1.2$ clusters in dendrites of hippocampal neurons.

To exclusively label $Ca_V1.2$ channels located in the plasma membrane, we transfected cultured hippocampal neurons with a $Ca_V1.2$ construct containing an HA tag in the extracellular loop adjacent to the transmembrane helix IIS5 ($Ca_V1.2$-HA) (Obermair et al., 2004). Cotransfection with soluble eGFP allowed identification of transfected neurons and revealed the morphology of the dendrites. If $Ca_V1.2$ channel clusters are maintained by an equilibrium of insertion of newly synthesized channels and the internalization and degradation of existing channels (Fig. 2*D*), $Ca_V1.2$-HA channels exposed at the membrane during a brief labeling period (pulse) will be replaced by newly inserted channels. Thus, surface-exposed labeled $Ca_V1.2$-HA channels should decline during the postincubation (chase) period.

To test this hypothesis, cultured hippocampal neurons (18–20 DIV) cotransfected with $Ca_V1.2$-HA and eGFP were incubated with anti-HA primary antibody for 10 min at 37°C and subsequently returned to glia-conditioned medium for various durations (0, 5, 15, 30, 60 min) before fixation with paraformaldehyde (Fig. 2*A*). Subsequently, immunolabeling of nonpermeabilized neurons with Alexa Fluor 594-conjugated secondary antibody resulted in the exclusive labeling of those channels, which were exposed at the membrane during the primary labeling period until the time of fixation. Internalized anti-HA-labeled $Ca_V1.2$-HA channels and newly inserted channels remained unlabeled. Figure 2*B* shows that at all examined time points $Ca_V1.2$-HA clusters are localized uniformly along the dendritic shaft and on the spines. Quantitative analysis of the cluster density and their fluorescence intensity in dendritic shafts and spines demonstrates that neither the number of labeled $Ca_V1.2$-HA in the clusters nor the total number of clusters in shafts and spines changed significantly over the 1 h observation period (Fig. 2*C*; 12–14 analyzed dendritic segments in three separate experiments; one-way ANOVA, $p = 0.17–0.88$). Thus, the turnover rate of $Ca_V1.2$ channels in clusters in dendrites of hippocampal neurons is well over 1 h, and the apparent stability of $Ca_V1.2$-HA is not achieved by a dynamic equilibrium of rapid internalization and insertion of calcium channels.

Block of dynamin-dependent endocytosis leads to a slow increase in $Ca_V1.2$-HA cluster density

The pulse–chase experiments described above demonstrated that at steady state, internalization and degradation of $Ca_V1.2$ channels do not result in detectable turnover of channels in clusters within 1 h. To tip the balance of membrane traffic, we next blocked endocytosis in cultured hippocampal neurons using Dynasore. This drug blocks endocytosis by specifically inhibiting the GTPase activity of dynamin (Newton et al., 2006; Jaskolski et al.,

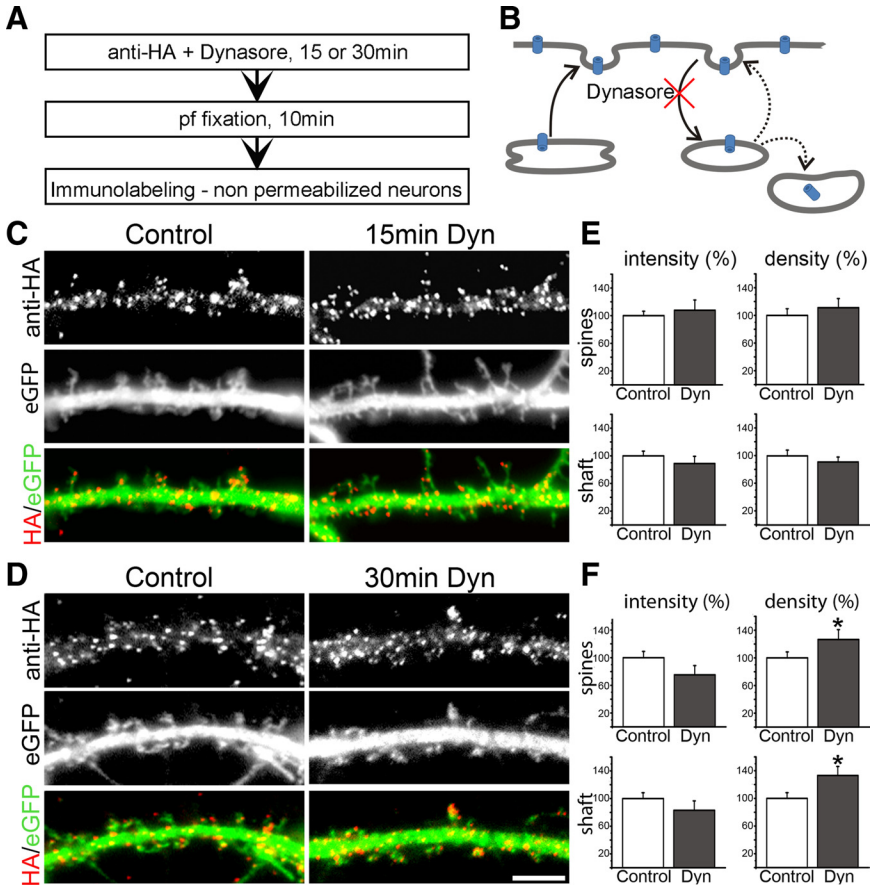

Figure 3. Blocking endocytosis leads to increased $Ca_V1.2$-HA cluster density after 30 min. ***A***, Experimental workflow. pf, Paraformaldehyde. ***B***, Dynasore blocks dynamin-dependent endocytosis and membrane recycling. ***C***, ***D***, Live cell staining of neurons cotransfected with $Ca_V1.2$-HA and eGFP shows that blocking endocytosis with 80 μM Dynasore (Dyn) for 15 and 30 min does not alter the labeling pattern of $Ca_V1.2$-HA clusters in dendritic shafts and spines. Scale bar, 5 μm. ***E***, ***F***, Quantification of $Ca_V1.2$-HA clusters indicates no significant change in clusters density and size after 15 min of Dynasore treatment, but a significant 26.6 ± 12.2% and 33.1 ± 11.8% increase of cluster density on shafts and spines after 30 min of Dynasore treatment (mean ± SEM; N = 23–31 analyzed dendritic segments in 3–4 separate experiments; *p = 0.02–0.05, significance, t test).

2009), which has recently been implicated in $Ca_V1.2$ turnover in neurons (Green et al., 2007). If the number of $Ca_V1.2$-HA channels in the dendritic membrane is regulated by the equilibrium of channel insertion and internalization, blocking endocytosis should increase membrane expression of $Ca_V1.2$-HA.

Living neurons transfected with $Ca_V1.2$-HA and eGFP were simultaneously incubated with anti-HA and 80 μM Dynasore for 15 and 30 min (Fig. 3*A*). After fixation and washing, surface $Ca_V1.2$-HA channels were visualized by immunolabeling in nonpermeabilized conditions. Blocking endocytosis did not change the overall distribution of $Ca_V1.2$-HA clusters in dendritic shafts and spines (Fig. 3*C*,*D*). For the 15 min time point, quantitative analysis showed that neither the fluorescence intensity of clusters nor the cluster density in dendritic shafts or spines was altered (Fig. 3*E*; 31–38 analyzed dendritic segments in four experiments; t test, $p = 0.18–0.31$). Only after 30 min of Dynasore treatment, quantification revealed a modest effect of blocking endocytosis. At this time point, $Ca_V1.2$-HA cluster density in the spines and in the shaft was increased by 26.6 ± 12.2% ($p = 0.046$) and 33.1 ± 11.8% ($p = 0.016$), respectively (Fig. 3*E*,*F*). Together, the lack of channel turnover in clusters during the 60 min pulse–chase experiment and the increase in $Ca_V1.2$-HA cluster density but not intensity upon 30 min Dynasore treatment suggest that channel trafficking does not contribute substantially to channel turnover within clusters, whereas blocking endocytosis favors the formation of new clusters, possibly because of a buildup of the mobile channel population outside the clusters.

$Ca_V1.2$-HA channels are not concentrated in recycling endosomes

In the postsynaptic compartment of neurons, constitutive trafficking by recycling endosomes is a major mechanism for membrane and protein turnover during basal conditions as well as for activity-induced changes of synaptic size and composition (Ehlers, 2000; Blanpied et al., 2002; Park et al., 2006). The observed changes in cluster density induced by 30 min Dynasore treatment (Fig. 3) may result either from buildup of newly synthesized channels or from recycling channels present in the endosomes before blocking endocytosis with Dynasore. Therefore, we examined whether recycling of membrane proteins is detectable in dendrites within this time and, if so, whether $Ca_V1.2$-HA channels can be detected in the endocytic compartments.

The use of fluorescently labeled transferrin is a method to monitor internalization of membrane receptors and a marker for recycling endosomes (Park et al., 2006). We incubated cultured hippocampal neurons with transferrin-Alexa Fluor 488 (Tf-488) for 30 min at 37°C and then stained the actin cytoskeleton with phalloidin-Alexa Fluor 594 to outline the morphology of the dendrites (Fig. 4*A*). Strong Tf-488 labeling throughout the dendrites indicated a considerable amount of membrane recycling during the 30 min incubation time (Fig. 4*B*). Consistent with a previous report by Park et al. (2006), we found that recycling vesicles are mainly localized along the dendritic shaft and less frequently on spines of hippocampal neurons.

To assess whether L-type calcium channels accumulate in recycling endosomes, we coincubated $Ca_V1.2$-HA transfected neurons with anti-HA and Tf-488 at 37° for 30 min and then fixed, permeabilized, and immunolabeled the neurons with Alexa Fluor 594-conjugated secondary antibody (Fig. 4*C*). If a significant portion of $Ca_V1.2$-HA would be subject to continuous recycling by similar mechanisms, $Ca_V1.2$-HA staining should colocalize with Tf-488 in recycling endosomes over time (Fig. 4*E*). The merged color image shows the typical distribution pattern of $Ca_V1.2$-HA surface clusters coexisting side-by-side with the typical pattern of Tf-488-labeled endocytic membrane compartments (Fig. 4*D*). For the most part the two proteins were not colocalized (the red and green structures are clearly separated from each other) and the endosomes were devoid of $Ca_V1.2$-HA labeling. At the rare sites of colocalization (yellow) the shapes of both structures differed from each other, suggesting that these events represent a random superposition of $Ca_V1.2$-HA clusters in the membrane with Tf-488 labeled endocytic compartments rather than colocalization of $Ca_V1.2$-HA and Tf-488 in recycling endosomes. Accordingly, correlation analysis gave a Pearson's coefficient of 0.18 ± 0.06 (mean ± SD, $n = 18$

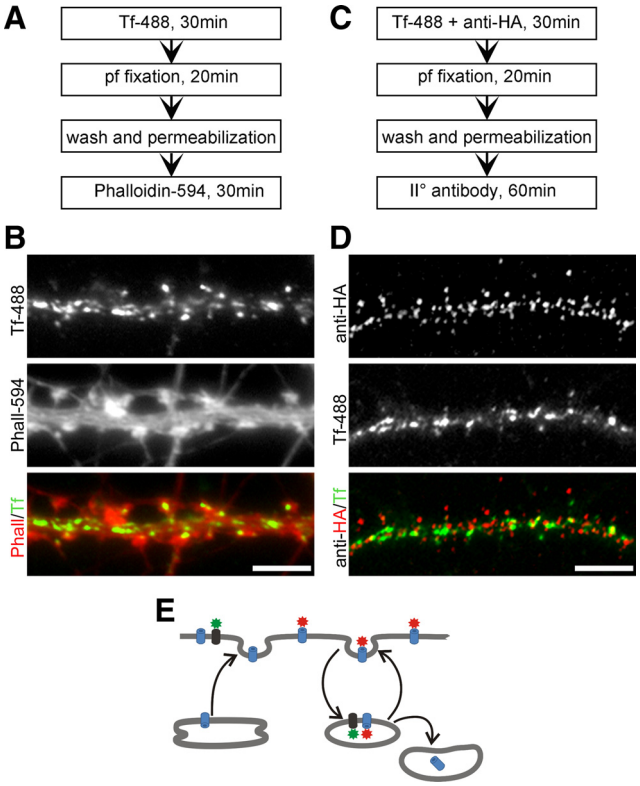

Figure 4. Clusters of $Ca_V1.2$-HA channels do not colocalize with Tf-488-labeled recycling endosomes. ***A***, ***C***, Experimental workflow. pf, Paraformaldehyde. ***B***, Hippocampal neurons incubated for 30 min with Tf-488 and subsequently labeled with phalloidin-Alexa Fluor 594 to outline dendritic spines shows abundant uptake of Tf-488 into endocytic compartments in the dendritic shaft and, to a lesser degree, in the spines. ***D***, Simultaneous incubation with Tf-488 and anti-HA and subsequent immunolabeling of permeabilized neurons demonstrates little to no colocalization of $Ca_V1.2$-HA and Tf-488 into endocytic compartments after 30 min. ***E***, If $Ca_V1.2$-HA (red) would be subject to rapid recycling, co-uptake with Tf-488 (green) would have been expected. Scale bars, 5 μm.

analyzed dendritic segments), indicating no correlation, and object-based analysis according to Bolte and Cordelières (2006) showed that only 7.2 ± 3.0% (mean ± SD, $n = 18$) of centers of mass of $Ca_V1.2$-HA clusters coincided with areas of Tf-488 labeled endosomal structures. Thus, surface-labeled $Ca_V1.2$-HA clusters do not include channels in recycling endosomes, and if the calcium channels undergo endocytic recycling, this occurs at densities below the level of detection of our sensitive immunolabeling protocol.

Single particle tracking reveals distinct dynamics of $Ca_V1.2$ channels in dendrites and axons

The slow turnover rates of clustered $Ca_V1.2$ channels correspond well to the major immobile channel fraction observed in FRAP experiments but do not explain the existence of the smaller yet significant mobile fraction. This mobile fraction might reflect channels moving laterally in the plane of the membrane. To resolve the dynamics of $Ca_V1.2$s in the membrane at high spatial and temporal resolution, we performed SPT experiments in living neurons transfected with $Ca_V1.2$-SEP or $Ca_V1.2$-HA.

To independently validate the functionality of the fusion constructs, we first analyzed $Ca_V1.2$-SEP and $Ca_V1.2$-HA in dysgenic myotubes. These $Ca_V1.1$-null mutant muscle cells can be functionally reconstituted with $Ca_V1.1$ or $Ca_V1.2$ (Flucher et al., 2000; Tuluc et al., 2007) and thus allow the rigorous analysis of targeting and current properties of L-type calcium channels in the native environment of a differentiated excitable cell. Both $Ca_V1.2$-SEP and $Ca_V1.2$-HA were localized in plasma membrane/sarcoplasmic reticulum junctions, indicating proper membrane expression and targeting (data not shown). Whole-cell patch-clamp analysis revealed calcium currents with similar biophysical properties but reduced current density of $Ca_V1.2$-SEP compared to $Ca_V1.2$-HA and the untagged channel (Fig. 5*C*,*D*). Reduced *On*-gating charges at test pulses to the reversal potential (data not shown) indicate that this is at least in part due to reduced membrane expression of the SEP-tagged channel. Nevertheless, in neurons SPT analysis of SEP- and HA-tagged $Ca_V1.2$ displayed identical frequency distributions of diffusion coefficients (Fig. 5*E*), comparable diffusion coefficients, and probability of confinement in dendrites and axons (Fig. 5*F*,*H*), indicating that the insertion of different tags in the channel does not adversely affect the channel mobility in the membrane.

Rat hippocampal neurons transfected with the HA- or SEP-tagged $Ca_V1.2$ were labeled with anti-HA and anti-rat QDs or anti-GFP QDs, respectively, at low labeling density to allow reconstruction of trajectories of individual channels over the entire observation period (1 min; acquisition rate, 30 Hz; Fig. 5*B*). Reconstructed trajectories where superimposed onto the corresponding image of the neurite labeled with a synaptic marker (Groc et al., 2006). Consistent with our published immunolabeling data, QD-labeled channels were frequently observed in the shaft and spines of dendrites. However, QD-labeled channels were also found in axons. In dendrites most of the trajectories were confined to small areas, indicative of little to no lateral diffusion during the 1 min recording time (Fig. 5*B*). In contrast, during 1 min $Ca_V1.2$ trajectories recorded in axons showed substantial lateral movement over several micrometers.

From the trajectories we calculated the mean square displacement. Based on the calculation of MSD, the instantaneous diffusion coefficient, the probability of confinement, and the explored surface area during confinement were analyzed. Both tagged $Ca_V1.2$ constructs showed clearly distinct mobilities in dendrites and axons. This difference is shown in the MSD plot over time (Fig. 5*F*) where the slope and curvature of the dendritic function reveals a confined motion. In contrast, the MSD plot of $Ca_V1.2$s in the axon is much steeper and almost linear, indicating less confined movement. Nevertheless, the diffusion of the channel in the axonal membrane is still slower than that of a known, freely diffusing, membrane-associated protein, GPI-GFP (Fig. 5*F*). The diffusion coefficients of $Ca_V1.2$-HA and $Ca_V1.2$-SEP in axons were 0.064 $\mu m^2\ s^{-1}$ and 0.043 $\mu m^2\ s^{-1}$, respectively (Fig. 5*G*; Table 1). Together, the dynamic properties of the axonal $Ca_V1.2$s are reminiscent of highly diffusive membrane proteins (Choquet and Triller, 2003). In dendrites, the average diffusion coefficients were about an order of magnitude lower than those in axons (Fig. 5*F*; Table 1), consistent with the confined mobility of the $Ca_V1.2$ channels indicated by the saturating MSD function (Fig. 5*F*). These differences of Ca_V mobility in axons and dendrites were further reflected in a low probability of confinement calculated for axonal channels ($Ca_V1.2$-HA 0.29 ± 0.05; $Ca_V1.2$-SEP 0.17 ± 0.03) (Fig. 5*H*), as opposed to a high probability of confinement of dendritic channels ($Ca_V1.2$-HA 0.61 ± 0.02; $Ca_V1.2$-SEP 0.63 ± 0.02). However, the range of diffusion coefficients of dendritic $Ca_V1.2$ trajectories was very wide (Fig. 5*G*), suggesting that $Ca_V1.2$ channels in dendrites exist in various dynamic states.

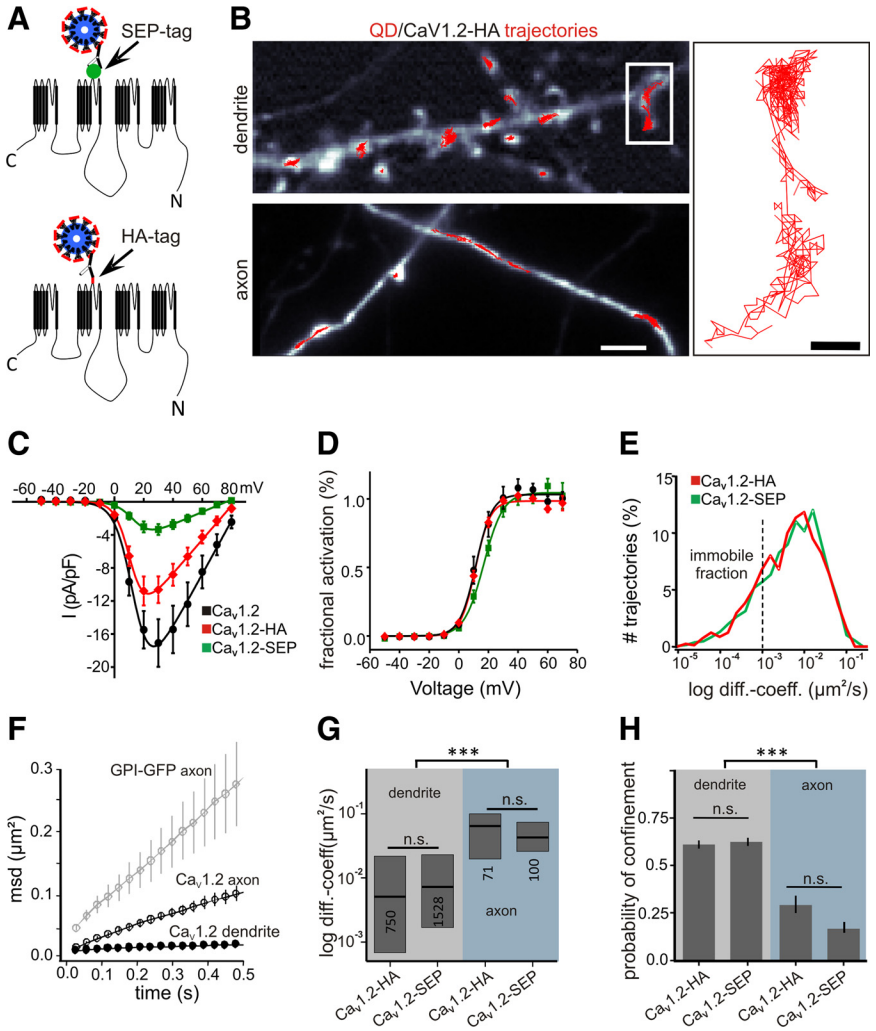

Figure 5. Single particle tracking of $Ca_V1.2$ in the cell surface of dendrites and axons of hippocampal neurons. ***A***, Membrane topology of $Ca_V1.2$ channels showing the position of the SEP-tag and HA-tag used for labeling with quantum dots. ***B***, Fluorescence images of a dendrite and an axon of a $Ca_V1.2$-HA and Homer1C-DsRed-cotransfected neuron (gray-scale image) with superimposed trajectories of individual QD-labeled $Ca_V1.2$-HA channels (red). Scale bar, 5 μm. Magnified trajectories (right) show that during the 60 s recording time, $Ca_V1.2$-HA is transiently confined in dendrites during periods of free diffusion. Scale bar, 1 μm. ***C***, ***D***, Comparison of current–voltage curves and voltage dependences of activation of untagged, HA-, and SEP-tagged $Ca_V1.2$ (black, red, green lines, respectively) expressed and recorded in dysgenic myotubes (mean ± SEM). ***E***, Distribution curves of the instantaneous diffusion coefficients of the SEP- and HA-tagged constructs are identical (mean ± SEM). ***F***, The mean square displacement curves indicate strongly confined movement in dendrites and diffusive movement of $Ca_V1.2$-SEP in axons; for comparison, note the MSD curve of the freely diffusive GPI-GFP in the axon. ***G***, The diffusion coefficients for both constructs are an order of magnitude lower in dendrites than axons ($HA\text{-}tag_{dendritic}$ = 0.005 $\mu m^2 s^{-1}$ IQR 0.0007/0.02; $SEP\text{-}tag_{dendritic}$ = 0.007 $\mu m^2 s^{-1}$ IQR 0.002/0.02; $HA\text{-}tag_{axonal}$ = 0.04 $\mu m^2 s^{-1}$ IQR 0.02/0.07; $SEP\text{-}tag_{axonal}$ = 0.06 $\mu m^2 s^{-1}$ IQR 0.02/0.1; Kruskal–Wallis test, followed by a Dunn's test, $p < 0.0001$). ***H***, The probability of confinement is significantly higher in dendrites than in axons (one-way ANOVA followed by a Newman–Keuls test, $p < 0.0001$).

Table 1. Diffusion coefficients of $Ca_V1.2$ channels in axons and dendrites of mature hippocampal neurons

	Axon			Dendrite		
Constructs	N^a	Diffusion coefficient^b ($\mu m^2 s^{-1}$)	IQR^c	N^a	Diffusion coefficient^b ($\mu m^2 s^{-1}$)	IQR^c
$Ca_V1.2$-HA	71	0.064	0.02/0.10	750	0.005	0.0007/0.02
$Ca_V1.2$-SEP	100	0.043	0.02/0.07	1528	0.007	0.002/0.02

[a]Number of trajectories.

[b]Median.

[c]Interquartile range (0.25–0.75).

SPT reveals two dynamic states of $Ca_V1.2$ channels in postsynaptic compartments of hippocampal neurons

Based on the results of our FRAP and live cell labeling experiments shown above, for dendrites the expectation would be to either find two independent populations of immobile and mobile $Ca_V1.2$ channels, or find $Ca_V1.2$ channels that can transit between a confined and a diffusive state.

Figure 6*A* shows dendrites of living hippocampal neurons transfected with $Ca_V1.2$-SEP (green) and the postsynaptic scaffold protein PSD95-mCherry (red). Trajectories of QD-labeled $Ca_V1.2$-SEP are superimposed in light blue. The majority of $Ca_V1.2$ trajectories colocalized with $Ca_V1.2$-SEP clusters (arrows) and to a lesser degree with postsynaptic densities (arrowheads; Di Biase et al. 2008). Closer inspection of the trajectories revealed two populations: (1) a major population of channels that did not leave the respective compartment and was classified as strongly confined (diffusion coefficient, <0.005 $\mu m^2 s^{-1}$) (Fig. 6*F–H*); and (2) a minor population of channels that alternated between periods of confinement and diffusion in the dendritic membrane (Fig. 6*I–K*). The latter mostly represented channels that also exchanged between the inside and outside of $Ca_V1.2$-SEP clusters (~35%) or postsynaptic densities (~10%) (Fig. 6*C*). The diffusion coefficients calculated separately for each state revealed one order of magnitude increase for channels in the diffusive state (Table 2). The example in Figure 6, *I–K*, shows a trajectory changing between periods of immobility (diffusion coefficient, <0.001 $\mu m^2 s^{-1}$), confinement (diffusion coefficient 0.0023 $\mu m^2 s^{-1}$), and diffusive states (diffusion coefficient 0.027 $\mu m^2 s^{-1}$). Immobile and highly confined mobility were preferentially observed inside $Ca_V1.2$-SEP clusters (Fig. 6*I*, yellow trajectories, numbers 1, 2 and 3), whereas the trajectory escaped the cluster during a phase of increased mobility (Fig. 6*I*, red trajectory). The distinct frequency distributions of diffusion coefficients also confirm that overall the fraction of diffusive trajectories is larger outside of $Ca_V1.2$-SEP clusters than inside (Fig. 6*B*). Furthermore, the average diffusion coefficient of trajectories outside $Ca_V1.2$-SEP clusters was twofold higher than that inside (Table 3). The observations that a subpopulation of channels spends part of their life time in a higher mobile state and that this preferentially occurs outside channel clusters is in good agreement with the size and distribution of mobile channels determined by our FRAP experiments.

Consistent with previous findings by us and others (Davare et al., 2001; Obermair et al., 2004; Di Biase et al., 2008), we observed

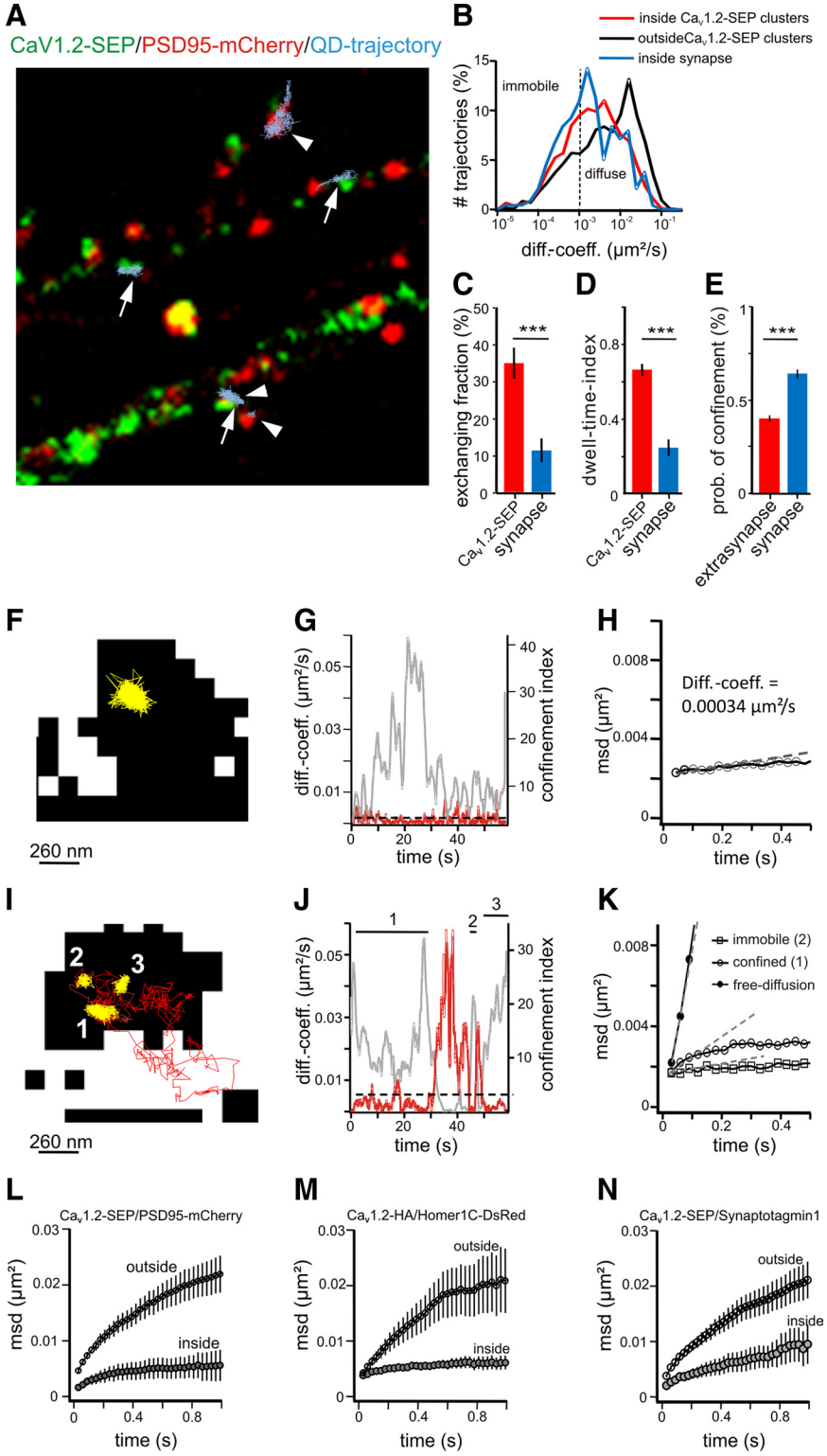

Figure 6. SPT analysis reveals highly confined and exchanging $Ca_V1.2$s in synaptic and extrasynaptic regions of dendrites. ***A***, Trajectories of QD-labeled $Ca_V1.2$-SEP channels (light blue; arrows/arrowheads) relative to clusters $Ca_V1.2$-SEP (green) and PSD95-mCherry (red) in dendrites of hippocampal neurons. Note that trajectories are confined and preferentially localized at $Ca_V1.2$-SEP clusters and/or PSD95-mCherry clusters. ***B***, Distribution of diffusion coefficients (diff.coeff.) of channels in synapses (blue trace, 527 trajectories $n_{cells} = 20$), $Ca_V1.2$-SEP clusters (red trace, 1315 trajectories, $n_{cells} = 20$), and outside clusters (black trace, 1073 trajectories, $n_{cells} = 20$) are significantly different (Mann–Whitney test, $p < 0.0001$). ***C***, ***D***, Fraction of channels exchanging between inside and outside of $Ca_V1.2$-SEP clusters (34.8 ± 4.2%, $n_{trajectories} = 447$, $n_{cell} = 23$ of three cultures) and PSD95-mCherry clusters (***C***) and their dwell time index in both compartments (***D***). ***E***, $Ca_V1.2$-HA probability of confinement in the synaptic and extrasynaptic compartments. ***F–H***, Example trajectory of a channel (yellow) in a $Ca_V1.2$-SEP cluster (black) (***F***) with diffusion coefficient (***G***, red) and MSD (***H***) characteristics for highly confined channels. ***I–K***, Example trajectory of a channel switching between phases of immobility (yellow, 2), confined mobility (yellow, 1, 3), and free diffusion (red) partially outside the $Ca_V1.2$-SEP cluster (black). Corresponding plot of diffusion coefficients (***J***, red) and MSD functions given for each mode (***K***). ***L–N***, MSD functions of channels relative to PSD95-mCherry (***L***), Homer1C-DsRed (***M***), and Synaptotagmin1-Oyster550 (***N***), are shown separately for trajectories inside and outside clusters of the respective synaptic marker.

a subset of $Ca_V1.2$ trajectories colocalized with synaptic markers in dendritic spines (Fig. 6*A*, arrowheads). The frequency distribution of diffusion coefficients (Fig. 6*B*) together with the increased probability of confinement of channels inside synapses (0.64 ± 0.022, $n = 431$ trajectories) compared to outside (0.40 ± 0.015, $n = 840$ trajectories) (Fig. 6*E*) indicate that synaptic channels mostly resemble the highly confined type. To explore the hypothesis that $Ca_V1.2$ channels are specifically anchored in postsynaptic signaling complexes (Davare et al., 2001; Oliveria et al., 2007), we cotransfected neurons with either $Ca_V1.2$-SEP and PDS95-mCherry (Fig. 6*L*) or $Ca_V1.2$-HA and Homer1C-DsRed (Fig. 6*M*), or we labeled $Ca_V1.2$-SEP transfected cultures with fluorescently labeled anti-Synaptotagmin1 (Fig. 6*N*). Analysis of the MSD inside and outside synapses for all three synaptic markers showed stronger confinement of channels within the PSD than outside. Also, the diffusion coefficients of channels inside synapses were approximately twofold lower than those outside, independent of the used synaptic marker (Table 3). Minor differences among the MSD plots and diffusion coefficients are most likely due to a different degree of colocalization of $Ca_V1.2$ with the used synaptic markers. The stronger confinement of $Ca_V1.2$-HA channels inside synapses was further reflected by the radius of the explored area of confinement calculated for confined channels inside and outside Homer clusters (inside Homer, $r = 44 \pm 5$ nm; outside Homer, $r = 75 \pm 3$ nm; $p < 0.0001$). The fact that extrasynaptic channels also showed a confined mobility was expected because $Ca_V1.2$-SEP clusters are not limited to synaptic locations. Interestingly, the differences in the mobility of channels inside and outside synapses are similar to those measured inside and outside of $Ca_V1.2$-SEP clusters. This is consistent with the notion that synaptic $Ca_V1.2$ channels are mostly clustered and that $Ca_V1.2$ clusters inside and outside synapses are not fundamentally different.

Table 2. Diffusion coefficients of dendritic $Ca_V1.2$ channels in confined or diffusive state

	Confined		Diffusive	
Constructs	Diffusion coefficient[a] ($\mu m^2 s^{-1}$)	IQR[b]	Diffusion coefficient[a] $\mu m^2 s^{-1}$	IQR[b]
$Ca_V1.2$-HA	0.0045	0.0020/0.0077	0.0205	0.0099/0.0396
$Ca_V1.2$-SEP	0.0044	0.0023/0.0075	0.0228	0.0126/0.0397

[a]Median.

[b]Interquartile range (0.25–0.75).

Table 3. Diffusion coefficients of $Ca_V1.2$ channels inside and outside of synapses and channel clusters

	Synaptic			Extrasynaptic		
Marker/constructs	N[a]	Diffusion coefficient[b] ($\mu m^2 s^{-1}$)	IQR[c]	N[a]	Diffusion coefficient[b] ($\mu m^2 s^{-1}$)	IQR[c]
PSD95/$Ca_V1.2$-SEP	148	0.0022	0.0005/0.0151	554	0.0054	0.0013/0.017
Homer/$Ca_V1.2$-HA	133	0.0043	0.0009/0.01041	546	0.0078	0.0017/0.0271
Stg/$Ca_V1.2$-SEP	249	0.00195	0.0008/0.0076	890	0.0048	0.0012/0.0202
	Inside cluster			Outside cluster		
$Ca_V1.2$-SEP	631	0.0026	0.0009/0.0079	1017	0.0047	0.0010/0.0202

[a]Number of trajectories.

[b]Median.

[c]Interquartile range (0.25–0.75).

Stg, Synaptotogmin.

Strong depolarization does not change the mobility of dendritic $Ca_V1.2$ channels

In young neurons, persistent depolarization with high potassium has been reported to downregulate L-type calcium currents and membrane expression of $Ca_V1.2$ within several minutes (Green et al., 2007). To examine whether such depolarization alters the fraction of mobile and immobile $Ca_V1.2$ channels or their overall mobility, we analyzed the dynamics of $Ca_V1.2$-SEP with FRAP and SPT in dendrites of mature hippocampal neurons (DIV 13–20) depolarized with 60 mM KCl (Fig. 7). After 15 min depolarization, the fluorescent recovery was indistinguishable from controls. The normalized FRAP curves showed the same initial rate of recovery and the same maximal degree of recovery after 15 min (Fig. 7*A*,*B*), indicating that the fraction of mobile and immobile $Ca_V1.2$ channels was not altered by continuous depolarization ($p = 0.73$, χ^2 test). Similarly, analysis of diffusion coefficients in SPT showed no persistent changes of channel mobility in response to depolarization. The diffusion coefficients inside and outside $Ca_V1.2$-SEP clusters were indistinguishable before and 5 or 15 min after a 90-s-long KCl (60 mM) depolarization (Fig. 7*C*). During the KCl depolarization, the diffusion coefficient of trajectories outside clusters was also indistinguishable from control; however, diffusion inside clusters was transiently reduced. Together, these experiments demonstrate that in dendrites of differentiated hippocampal neurons, strong depolarization with high KCl did neither change the fraction of mobile and immobile $Ca_V1.2$ channels nor their diffusion properties. If anything, KCl depolarization may transiently increase the stability of clustered $Ca_V1.2$-SEP channels.

In young (DIV 7) hippocampal neurons, FRAP analysis revealed an increased fraction of mobile channels under basal conditions. Fifteen minutes after photobleaching, recovery of $Ca_V1.2$-SEP fluorescence was about twice as high as that in mature neurons, reaching on average 62 ± 8% (Fig. 7*B*, mean ± SEM). Also, the diffusion coefficients of $Ca_V1.2$-HA determined

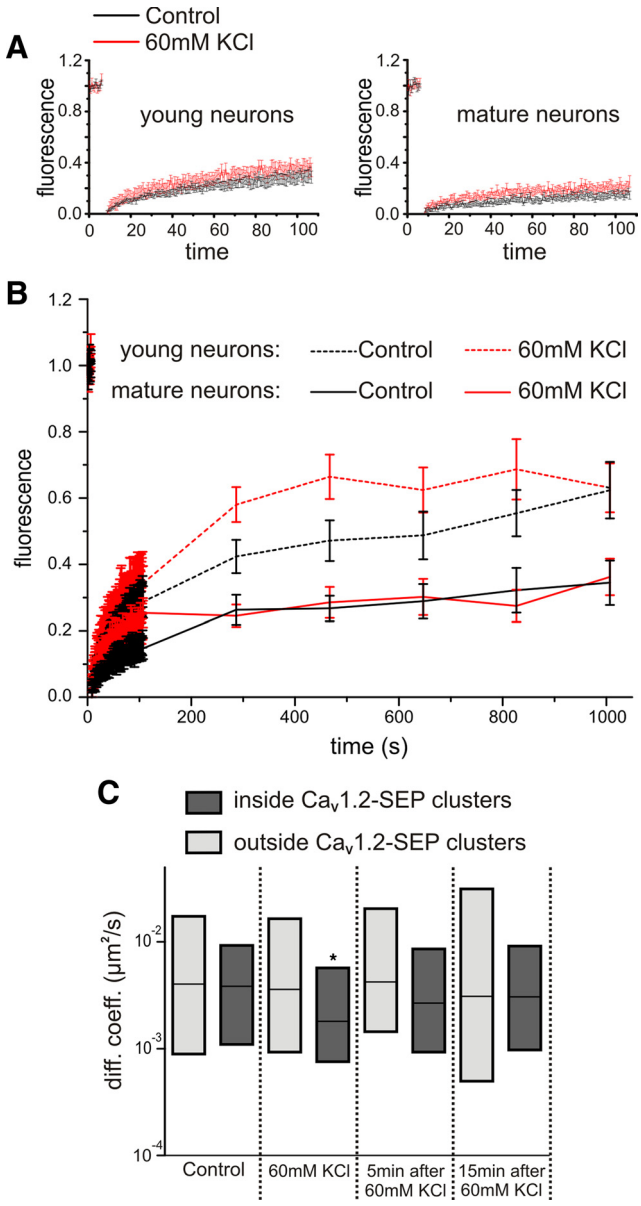

Figure 7. Dynamic properties of $Ca_V1.2$-SEP show little to no changes upon high KCl depolarization. ***A***, ***B***, Hippocampal neurons (DIV 7 and DIV 13–20) transfected with $Ca_V1.2$-SEP were exposed to 60 mM KCl containing (red) or normal Tyrode's solution (black) and analyzed with FRAP 15 min later. First 120 s were sampled at 1.5 Hz (***A***), then further images were captured every 3 min for 15 min (***B***, normalized means ± SEM). ***C***, Diffusion coefficients (diff. coeff.) of SPT trajectories inside (dark gray) and outside (light gray) $Ca_V1.2$-SEP clusters were recorded before depolarization (control), during 60 mM KCl treatment, 5 and 15 min after KCl depolarization. Box plots: median, IQR; *$p < 0.05$, *t* test.

in SPT experiments were significantly higher in 7-d-old young neurons (0.0168 $\mu m^2 s^{-1}$; IQR, 0.003/0.05; $n = 3$ neurons) compared to mature neurons (0.00511 $\mu m^2 s^{-1}$; IQR, 0.0007/0.02). Thus, during maturation $Ca_V1.2$ appears to be increasingly stabilized. Interestingly, although at the end of the recording period the mobile $Ca_V1.2$-SEP fraction in KCl-depolarized neurons is similar to that in the control, the rate of recovery as seen at the 5 and 8 min time points is increased in 60 mM KCl ($p = 0.0399$ and 0.0426, respectively). Therefore, persistent depolarization increased the lateral mobility of $Ca_V1.2$-SEP in dendrites of young but not of mature neurons.

Discussion

$Ca_V1.2$ LTCCs are expressed in the soma and dendrites of CNS neurons and function in activity-dependent signaling to the nucleus, synaptic plasticity, and the formation of long term memory. Conversely, membrane expression of $Ca_V1.2$ itself is regulated by activity, and their internalization may protect neurons from calcium-induced excitotoxicity and neurodegenerative disease. Here we employed various live cell labeling protocols, FRAP analysis, and SPT to determine the turnover and dynamics of $Ca_V1.2$ channels in dendrites at high temporal and spatial resolution. Our results demonstrate that the majority of dendritic $Ca_V1.2$s exists in stable clusters that turn over at low rates and show little or no lateral movement in the plane of the membrane. However, our FRAP and SPT analysis also revealed a previously unnoticed population of mobile channels, mostly outside of the clusters, that may be involved in maintaining the equilibrium of channels in synaptic and extrasynaptic $Ca_V1.2$ signaling complexes.

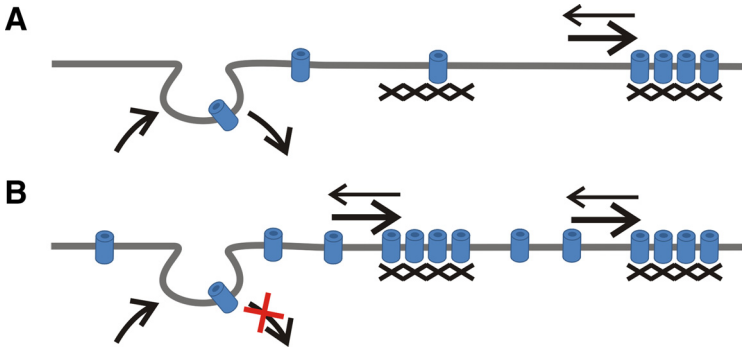

Figure 8. Model of the distribution and dynamics of $Ca_V1.2$ channels in dendrites of CNS neurons. The majority of channels are clustered in signaling complexes with a fixed number of channel slots. Outside of clusters, mobile channels are diffusely distributed. Membrane insertion and internalization causes a constant turnover of the diffuse channel population at a rate of about 1 h. Although $Ca_V1.2$s do exchange between the clustered and the diffuse state, this exchange appears to occur at much lower rates, such that basal turnover (***A***) does not result in a detectable exchange of clustered channels within 1 h. However, a build up of channels after blocking endocytosis (***B***) leads to the formation of new clusters within 30 min. Consequently, a reduction of channels—for example by increased endocytosis—is expected to first reduce the density of diffuse channels and later the dispersion of the channels clustered in $Ca_V1.2$ signaling complexes.

Multiple lines of new evidence support the conclusion that $Ca_V1.2$ channels primarily exist in stable clusters in the soma, dendrites, and dendritic spines of hippocampal neurons. In the pulse–chase experiments the number and size of $Ca_V1.2$ clusters did not decline over 1 h after live cell labeling of surface-exposed channels. Within half an hour $Ca_V1.2$ channels did not appear in recycling endosomes or other TfR-labeled endocytic structures, and blocking dynamin-dependent endocytosis resulted in a detectable increase of $Ca_V1.2$ cluster density only after 30 min. In FRAP experiments bleached $Ca_V1.2$-SEP clusters did not recover within 20 min, and SPT revealed a dominant population of highly confined $Ca_V1.2$ channels preferentially located in $Ca_V1.2$-SEP clusters and synapses. Together, these data indicate that in differentiated hippocampal neurons under basal conditions clustered $Ca_V1.2$s have a turnover rate greater than1 h. At this rate, channel internalization or recycling of this $Ca_V1.2$ population cannot possibly account for the activity-induced downregulation of L-type calcium currents observed within minutes after strong KCl depolarization or glutamate treatment (Green et al., 2007; Tsuruta et al., 2009). As in these studies activity- and glutamate-induced internalization had only been studied in Neuro2A cells and young cortical neurons and was not specific to $Ca_V1.2$ channels, it may be a developmental phenomenon no longer effective in differentiated neurons. Indeed, we observed increased mobility of $Ca_V1.2$ channels in 7-d-old hippocampal neurons, both with FRAP and SPT analysis. In hippocampal neurons that have differentiated mature features like dendritic spines, form extensive synapses, and show high spontaneous activity, the activity-dependent downregulation of ion channels may already have taken place. This notion is further supported by our present result showing that in mature neurons KCl depolarization did not alter the dynamics of $Ca_V1.2$ in FRAP and SPT experiments, as well as by previous findings showing that surface-expressed $Ca_V1.2$-HA clusters were not reduced in size or density after activation of NMDA receptors (Di Biase et al., 2008).

In addition to the stably clustered channels, our FRAP analysis provides experimental evidence for the existence of mobile $Ca_V1.2$ channels. In dendrites of differentiated hippocampal neurons they represented ~20% of membrane-expressed $Ca_V1.2$-SEP. The observation that fluorescence recovery was not accompanied by a reappearance of fluorescence in the clusters indicated that these mobile channels exist predominantly outside the clusters. KCl depolarization did not reduce the fraction of mobile channels. While these channels may be subject to higher turnover rates than clustered channels, in the spontaneously active, mature neurons their fractional content may already be at its lower limit, not allowing any further activity-induced downregulation of calcium currents. A coexistence of stably clustered and mobile diffuse $Ca_V1.2$ correlated well with our SPT results. There, the stably clustered channels are represented by the predominant fraction of highly confined channels with diffusion coefficients minor of 0.005 $\mu m^2 s^{-1}$. As expected, these were more frequent inside $Ca_V1.2$-SEP clusters and synapses. The mobile fraction most likely represents the transient diffusive states of the exchanging $Ca_V1.2$ population when escaping the clusters.

Interestingly, the MSD functions of the confined and the diffusive channel populations were saturating, indicating that in dendrites $Ca_V1.2$ channels inside and outside of clusters were confined in their lateral mobility. This is in stark contrast to $Ca_V1.2$ channels in axons where the diffusion coefficients, MSD functions, and the low probability of confinement indicated that $Ca_V1.2$s are highly diffusive. Thus, in the somatodendritic compartment $Ca_V1.2$ channels associate with binding partners that restrict their lateral mobility differentially within and outside of clusters. Although several interaction partners and binding sites for scaffold proteins have been identified in $Ca_V1.2$ (Altier et al., 2002; Weick et al., 2003; Malik et al., 2006), the specific scaffold proteins responsible for the clustering and immobilization of $Ca_V1.2$ channels in the postsynaptic membrane of hippocampal neurons remain to be identified. In axons of mature hippocampal neurons from which $Ca_V1.2$ channels are mostly excluded (Obermair et al., 2004), the channels apparently do not strongly interact with intracellular scaffolds or cytoskeletal proteins and thus remain freely mobile.

Together, our analysis of the turnover and dynamics of $Ca_V1.2$ channels in dendrites of hippocampal neurons suggest a model according to which channels inside and outside of clusters may exist in a dynamic equilibrium (Fig. 8). The emergence of new clusters within 30 min of blocking endocytosis demonstrates that

channel turnover in the membrane does occur on an hour timescale and also contributes to the formation of $Ca_V1.2$ clusters. However, the lower turnover rates of channels in existing clusters together with their extremely low diffusion rates indicate that in the clusters $Ca_V1.2$s are tightly anchored. Apparently, under basal conditions balanced insertion and internalization mostly causes turnover of diffuse mobile channels, whereas exchange with clustered channels remains negligible. However, when channels accumulate in the membrane due to an imbalance of insertion and internalization, new clusters are formed.

The observation that upon blocking endocytosis the density of clusters but not their size increased suggests that the number of channels in a cluster must be limited by a fixed number of anchoring sites so that additional channels in the membrane are not added to existing clusters but form new ones. Thus, like presynaptic neurotransmitter release sites, postsynaptic $Ca_V1.2$ signaling complexes may be limited in size by the number of calcium channel slots (Cao and Tsien, 2010) and the extent of their calcium nanodomain. Lately, we observed a similar increase in cluster density without concomitant increase in the fluorescence intensity of $Ca_V1.2$ channels in which the C-terminal PDZ protein binding site had been deleted (Di Biase et al., 2008). This similarity of effects is consistent with a role of the PDZ binding motif in endocytotic degradation of channels, as has been shown for G protein-coupled receptors (Trejo, 2005). A turnover mechanism by which entire clusters are rapidly formed or dissolved—presumably by exchange with the diffuse population—is also supported by an observation made when $Ca_V1.2$-SEP clusters were monitored over 20 min in living neurons. Although the great majority of clusters neither changed their position nor their labeling intensity, some new clusters appeared and some existing clusters disappeared within this period. Alternatively, the disappearing or newly appearing clusters might represent recycling channels (Green et al., 2007). In fact, in dendrites of hippocampal neurons, recycling endosomes turn over in $<$30 min and take up the GluR1 subunit of AMPA receptors (Kennedy et al., 2010). However, in light of the almost complete absence of co-uptake of Tf-488 and $Ca_V1.2$-HA within 30 min, it is rather unlikely that $Ca_V1.2$ channels participate in this recycling process.

$Ca_V1.2$ clusters are evenly distributed throughout the dendritic shafts and spines, where they show some overlap but no specific colocalization with synapses (Obermair et al., 2004; Di Biase et al., 2008). Accordingly, in SPT, highly confined $Ca_V1.2$s were found in synaptic as well as in extrasynaptic locations. This is different from the distribution and dynamics of NMDA receptors, which are aggregated and comparatively immobile in the postsynaptic domain but diffuse and mobile in extrasynaptic domains. In the case of $Ca_V1.2$ the average mobility of synaptic channels was only twofold lower than that of extrasynaptic channels. The diffusion coefficient of $Ca_V1.2$ in dendrites is about one order of magnitude lower than that of AMPA receptors (Bats et al., 2007; Heine et al., 2008) but similar to that reported for NMDA receptors (Groc et al., 2006). Interestingly, $Ca_V1.2$ channels and NMDA receptors share important scaffolds and downstream signaling proteins like AKAP79/150, CaMKII, PKA, and calcineurin (Oliveria et al., 2007), as well as functions in activity-dependent nuclear signaling and long-term synaptic plasticity (Graef et al., 1999; Weick et al., 2003; Lee et al., 2009; Rose et al., 2009). Thus, it is intriguing to speculate that immobilization in their respective signaling complexes may be important for the normal function of $Ca_V1.2$ (and NMDA receptors) in activating calcium-dependent signaling cascades. The dispersed distribution of $Ca_V1.2$ clusters independent of synapses corresponds well with their activation by global depolarization rather than by focally released neurotransmitter as well as their involvement in homeostatic plasticity (Rose et al., 2009; Goold and Nicoll, 2010). Calcium nanodomains in the vicinity of the clustered channels may enable the efficient activation of downstream signaling proteins, while their spatial separation from the NMDA receptors may be necessary to separate their molecularly similar but functionally distinct signaling pathways.

References

Altier C, Dubel SJ, Barrère C, Jarvis SE, Stotz SC, Spaetgens RL, Scott JD, Cornet V, De Waard M, Zamponi GW, Nargeot J, Bourinet E (2002) Trafficking of L-type calcium channels mediated by the postsynaptic scaffolding protein AKAP79. J Biol Chem 277:33598–33603.

Ashby MC, Ibaraki K, Henley JM (2004) It's green outside: tracking cell surface proteins with pH-sensitive GFP. Trends Neurosci 27:257–261.

Barria A, Malinow R (2005) NMDA receptor subunit composition controls synaptic plasticity by regulating binding to CaMKII. Neuron 48:289–301.

Bats C, Groc L, Choquet D (2007) The interaction between Stargazin and PSD-95 regulates AMPA receptor surface trafficking. Neuron 53:719–734.

Blanpied TA, Scott DB, Ehlers MD (2002) Dynamics and regulation of clathrin coats at specialized endocytic zones of dendrites and spines. Neuron 36:435–449.

Bolte S, Cordelières FP (2006) A guided tour into subcellular colocalization analysis in light microscopy. J Microsc 224:213–232.

Cao YQ, Tsien RW (2010) Different relationship of N- and P/Q-type Ca^{2+} channels to channel-interacting slots in controlling neurotransmission at cultured hippocampal synapses. J Neurosci 30:4536–4546.

Chan CS, Guzman JN, Ilijic E, Mercer JN, Rick C, Tkatch T, Meredith GE, Surmeier DJ (2007) 'Rejuvenation' protects neurons in mouse models of Parkinson's disease. Nature 447:1081–1086.

Charrier C, Machado P, Tweedie-Cullen RY, Rutishauser D, Mansuy IM, Triller A (2010) A crosstalk between beta1 and beta3 integrins controls glycine receptor and gephyrin trafficking at synapses. Nat Neurosci 13:1388–1395.

Choquet D, Triller A (2003) The role of receptor diffusion in the organization of the postsynaptic membrane. Nat Rev Neurosci 4:251–265.

Clark NC, Nagano N, Kuenzi FM, Jarolimek W, Huber I, Walter D, Wietzorrek G, Boyce S, Kullmann DM, Striessnig J, Seabrook GR (2003) Neurological phenotype and synaptic function in mice lacking the CaV1.3 alpha subunit of neuronal L-type voltage-dependent Ca^{2+} channels. Neuroscience 120:435–442.

Davare MA, Avdonin V, Hall DD, Peden EM, Burette A, Weinberg RJ, Horne MC, Hoshi T, Hell JW (2001) A beta2 adrenergic receptor signaling complex assembled with the Ca^{2+} channel Cav1.2. Science 293:98–101.

Day M, Wang Z, Ding J, An X, Ingham CA, Shering AF, Wokosin D, Ilijic E, Sun Z, Sampson AR, Mugnaini E, Deutch AY, Sesack SR, Arbuthnott GW, Surmeier DJ (2006) Selective elimination of glutamatergic synapses on striatopallidal neurons in Parkinson disease models. Nat Neurosci 9:251–259.

Deisseroth K, Mermelstein PG, Xia H, Tsien RW (2003) Signaling from synapse to nucleus: the logic behind the mechanisms. Curr Opin Neurobiol 13:354–365.

Di Biase V, Obermair GJ, Szabo Z, Altier C, Sanguesa J, Bourinet E, Flucher BE (2008) Stable membrane expression of postsynaptic CaV1.2 calcium channel clusters is independent of interactions with AKAP79/150 and PDZ proteins. J Neurosci 28:13845–13855.

Dolmetsch R (2003) Excitation-transcription coupling: signaling by ion channels to the nucleus. Sci STKE 2003:PE4.

Dresbach T, Hempelmann A, Spilker C, tom Dieck S, Altrock WD, Zuschratter W, Garner CC, Gundelfinger ED (2003) Functional regions of the presynaptic cytomatrix protein bassoon: significance for synaptic targeting and cytomatrix anchoring. Mol Cell Neurosci 23:279–291.

Ehlers MD (2000) Reinsertion or degradation of AMPA receptors determined by activity-dependent endocytic sorting. Neuron 28:511–525.

Flucher BE, Andrews SB, Fleischer S, Marks AR, Caswell A, Powell JA (1993) Triad formation: organization and function of the sarcoplasmic reticulum calcium release channel and triadin in normal and dysgenic muscle in vitro. J Cell Biol 123:1161–1174.

Flucher BE, Kasielke N, Gerster U, Neuhuber B, Grabner M (2000) Inser-

tion of the full-length calcium channel alpha(1S) subunit into triads of skeletal muscle in vitro. FEBS Lett 474:93–98.

Goold CP, Nicoll RA (2010) Single-cell optogenetic excitation drives homeostatic synaptic depression. Neuron 68:512–528.

Goslin K, Banker G (1998) Culturing nerve cells, Ed 2. Cambridge, MA: MIT.

Graef IA, Mermelstein PG, Stankunas K, Neilson JR, Deisseroth K, Tsien RW, Crabtree GR (1999) L-type calcium channels and GSK-3 regulate the activity of NF-ATc4 in hippocampal neurons. Nature 401:703–708.

Green EM, Barrett CF, Bultynck G, Shamah SM, Dolmetsch RE (2007) The tumor suppressor eIF3e mediates calcium-dependent internalization of the L-type calcium channel CaV1.2. Neuron 55:615–632.

Groc L, Heine M, Cousins SL, Stephenson FA, Lounis B, Cognet L, Choquet D (2006) NMDA receptor surface mobility depends on NR2A–2B subunits. Proc Natl Acad Sci U S A 103:18769–18774.

Heine M, Groc L, Frischknecht R, Béïque JC, Lounis B, Rumbaugh G, Huganir RL, Cognet L, Choquet D (2008) Surface mobility of postsynaptic AMPARs tunes synaptic transmission. Science 320:201–205.

Hell JW, Westenbroek RE, Warner C, Ahlijanian MK, Prystay W, Gilbert MM, Snutch TP, Catterall WA (1993) Identification and differential subcellular localization of the neuronal class C and class D L-type calcium channel alpha 1 subunits. J Cell Biol 123:949–962.

Jaskolski F, Mayo-Martin B, Jane D, Henley JM (2009) Dynamin-dependent membrane drift recruits AMPA receptors to dendritic spines. J Biol Chem 284:12491–12503.

Kasielke N, Obermair GJ, Kugler G, Grabner M, Flucher BE (2003) Cardiac-type EC-coupling in dysgenic myotubes restored with Ca^{2+} channel subunit isoforms alpha1C and alpha1D does not correlate with current density. Biophys J 84:3816–3828.

Kennedy MJ, Davison IG, Robinson CG, Ehlers MD (2010) Syntaxin-4 defines a domain for activity-dependent exocytosis in dendritic spines. Cell 141:524–535.

Korenkov AI, Pahnke J, Frei K, Warzok R, Schroeder HW, Frick R, Muljana L, Piek J, Yonekawa Y, Gaab MR (2000) Treatment with nimodipine or mannitol reduces programmed cell death and infarct size following focal cerebral ischemia. Neurosurg Rev 23:145–150.

Lee SJ, Escobedo-Lozoya Y, Szatmari EM, Yasuda R (2009) Activation of CaMKII in single dendritic spines during long-term potentiation. Nature 458:299–304.

Malik K, Hall DD, Hell JW (2006) Interaction of alpha actinin with the L-type calcium channel (Cav1.2). Soc Neurosci Abstr 32:131.8.

Miesenböck G, De Angelis DA, Rothman JE (1998) Visualizing secretion and synaptic transmission with pH-sensitive green fluorescent proteins. Nature 394:192–195.

Moosmang S, Haider N, Klugbauer N, Adelsberger H, Langwieser N, Müller J, Stiess M, Marais E, Schulla V, Lacinova L, Goebbels S, Nave KA, Storm DR, Hofmann F, Kleppisch T (2005) Role of hippocampal Cav1.2 Ca^{2+} channels in NMDA receptor-independent synaptic plasticity and spatial memory. J Neurosci 25:9883–9892.

Newton AJ, Kirchhausen T, Murthy VN (2006) Inhibition of dynamin completely blocks compensatory synaptic vesicle endocytosis. Proc Natl Acad Sci U S A 103:17955–17960.

Obermair GJ, Kaufmann WA, Knaus HG, Flucher BE (2003) The small conductance Ca^{2+}-activated K^+ channel SK3 is localized in nerve terminals of excitatory synapses of cultured mouse hippocampal neurons. Eur J Neurosci 17:721–731.

Obermair GJ, Szabo Z, Bourinet E, Flucher BE (2004) Differential targeting of the L-type Ca^{2+} channel alpha 1C (CaV1.2) to synaptic and extrasynaptic compartments in hippocampal neurons. Eur J Neurosci 19: 2109–2122.

Oliveria SF, Dell'Acqua ML, Sather WA (2007) AKAP79/150 anchoring of calcineurin controls neuronal L-type Ca^{2+} channel activity and nuclear signaling. Neuron 55:261–275.

Park M, Salgado JM, Ostroff L, Helton TD, Robinson CG, Harris KM, Ehlers MD (2006) Plasticity-induced growth of dendritic spines by exocytic trafficking from recycling endosomes. Neuron 52:817–830.

Rose J, Jin SX, Craig AM (2009) Heterosynaptic molecular dynamics: locally induced propagating synaptic accumulation of CaM kinase II. Neuron 61:351–358.

Sankaranarayanan S, De Angelis D, Rothman JE, Ryan TA (2000) The use of pHluorins for optical measurements of presynaptic activity. Biophys J 79:2199–2208.

Saxton MJ (1995) Single-particle tracking: effects of corrals. Biophys J 69:389–398.

Schlick B, Flucher BE, Obermair GJ (2010) Voltage-activated calcium channel expression profiles in mouse brain and cultured hippocampal neurons. Neuroscience 167:786–798.

Schurr A (2004) Neuroprotection against ischemic/hypoxic brain damage: blockers of ionotropic glutamate receptor and voltage sensitive calcium channels. Curr Drug Targets 5:603–618.

Sergé A, Fourgeaud L, Hémar A, Choquet D (2002) Receptor activation and homer differentially control the lateral mobility of metabotropic glutamate receptor 5 in the neuronal membrane. J Neurosci 22:3910–3920.

Stanika RI, Villanueva I, Pivovarova NB, Andrews SB (2010) Equivalent calcium loading via NMDA receptors or voltage-gated calcium channels induces similar toxicity in hippocampal neurons. Soc Neurosci Abstr 36:59.13.

Tanabe T, Beam KG, Adams BA, Niidome T, Numa S (1990) Regions of the skeletal muscle dihydropyridine receptor critical for excitation-contraction coupling. Nature 346:567–569.

Trejo J (2005) Internal PDZ ligands: novel endocytic recycling motifs for G protein-coupled receptors. Mol Pharmacol 67:1388–1390.

Tsuruta F, Green EM, Rousset M, Dolmetsch RE (2009) PIKfyve regulates CaV1.2 degradation and prevents excitotoxic cell death. J Cell Biol 187:279–294.

Tuluc P, Kern G, Obermair GJ, Flucher BE (2007) Computer modeling of siRNA knockdown effects indicates an essential role of the Ca^{2+} channel alpha2delta-1 subunit in cardiac excitation-contraction coupling. Proc Natl Acad Sci U S A 104:11091–11096.

Weick JP, Groth RD, Isaksen AL, Mermelstein PG (2003) Interactions with PDZ proteins are required for L-type calcium channels to activate cAMP response element-binding protein-dependent gene expression. J Neurosci 23:3446–3456.